Applied Thermal Engineering 231 (2023) 121005

Contents lists available at ScienceDirect

Applied Thermal Engineering

journal homepage: www.elsevier.com/locate/apthermeng

High-performance thermal management system for high-power LEDs based on double-nozzle spray cooling

Linyi Xiang, Yanhua Cheng, Xingjian Yu, Yiwen Fan, Xuan Yang, Xinfeng Zhang, Bin Xie, Xiaobing Luo *

School of Energy and Power Engineering, Huazhong University of Science and Technology, Wuhan 430074, PR China

ARTICLE INFO

Keywords:
Spray cooling
High-power LEDs
Nozzle configuration

ABSTRACT

Thermal management is one of the main challenges for high-power LEDs. As one of the state-of-the-art thermal management approaches, spray cooling can meet the requirements of fast cooling speed, large heat transfer coefficient, and less energy consumption when it provides thermal management for electronics with high heat flux. In this study, a high-performance spray cooling system for high-power LEDs is designed and established. The influence of nozzle configuration, flow rate, and nozzle-to-surface distance on the heat transfer characteristics are experimentally and numerically investigated. The system shows excellent heat dissipation capacity. Two different nozzle configurations are compared and the results show that the double-nozzle configuration possesses the highest single-phase heat transfer coefficient, reaching up to 20.7 kW/m^2·K with the flow rate of 150 mL/min. Interestingly, double-nozzle, which owns better heat transfer performance compared to single-nozzle, shows worse temperature uniformity inside the testing module. Simultaneously, the junction temperature of double-nozzle at the center chip can also be controlled to 85 °C corresponding to a 10% reduction for single-nozzle. The proposed cooling system may enable the further application of spray cooling in electronics like high-power LEDs, potentially reducing the energy consumption in cooling electronics and promoting the utilization of low-grade thermal energy.

1. Introduction

Light-emitting diodes (LEDs) are widely used around the world due to their long lifetime and eco-friendliness. The past few decades have witnessed significant breakthroughs in the material, packaging, and design of LEDs [1–2], which is developing in the trends of miniaturization and high-density packaging. The heating power of high-power LEDs can account for 60%-70% of the input electric power due to the nonradiative recombination with the MQW (Multiple Quantum Well) layer and light confinement within the LEDs packaging, which will lead to a sharp temperature rise of the device [3]. As a result, luminous flux degradation, wavelength drift, lifetime reduction, and even irreversible damage will occur in LEDs [4]. Therefore, thermal management is critical for high-power LEDs [5–6].

The local heat flux level of high-power LEDs can reach 500 W/cm^2 and the junction temperature should be controlled below 120 °C [7–8]. Limited by the packaging constrains, thermal characteristics, and materials factors, the forced air convection or passive liquid cooling methods [9–12] fail to meet the heat dissipation requirement of high-power LEDs, while active liquid cooling technology can due to its better heat transfer performance [13–14]. Active liquid cooling technologies, including microchannel liquid cooling, jet impingement liquid cooling, and spray cooling, have been widely studied [15–16]. Microchannel liquid cooling and jet impingement liquid cooling have shown excellent thermal management capacity in low-power LEDs (0.05 W to 1 W, micro/milli amps) but are not suitable for high-power LEDs (3 W or even tens of watts, several amperes) [17–25]. Spray cooling, regarded as the promising thermal management solution for ultra-high heat flux (>1000 W/cm^2) electronic devices has drawn tremendous attention, of which the studies focus on revealing the heat transfer mechanism, enhancing the heat dissipation capacity, and promoting the applications [26–28]. The flow parameters and nozzle configuration have been proven to have a significant influence on the heat transfer performance of spray cooling. Meanwhile, as an advanced thermal management method, spray cooling has been successfully applied to many fields, such as aerospace equipment [29], motor [30], and lithium-ion battery [31] while studies on spray cooling of LEDs are very limited. Only a few

* Corresponding author.
E-mail address: Luoxb@hust.edu.cn (X. Luo).

https://doi.org/10.1016/j.applthermaleng.2023.121005
Received 25 November 2022; Received in revised form 22 April 2023; Accepted 16 June 2023
Available online 17 June 2023

Nomenclature

C_p	heat capacity
D	spray area diameter
d_{32}	Sauter mean diameter
H	nozzle-to-surface distance
h	heat transfer coefficient
k	thermal conductivity
ΔP	pressure drop across nozzle
Q	Flow rate
$\overline{Q}''$	spray volumetric flux
q''	heat flux
R	stagnation point
T	temperature
t	time
$\overline{T}$	average temperature
T_{in}	inlet coolant temperature
ΔT_{uni}	temperature non-uniformity
u	droplet velocity
y	y coordinate
y_1	distance between T_{s1} and T_{21}
y_2	distance between T_{s2} and T_{23}

Greek symbols

θ	spray angle
ρ	density
σ	uncertainty

Subscripts

f	liquid
in	inlet
J	Junction
s	spray
s_1	substrate
s_2	surface

Abbreviations

LEDs	light-emitting diodes
SMD	Sauter mean diameter

studies take advantage of single nozzle spray cooling for the thermal management of LEDs and the effectiveness has been verified [32–33]. However, high-power LEDs is a temperature-sensitive optical device that requires high heat transfer coefficient throughout the whole surface. A single spray may not provide sufficient surface coverage for LEDs' unique shape and packaging constrains while double spray can cover a larger surface area. In order to explore how to integrate laboratory spray cooling systems with industrial applications, the coupling effect of various parameters and the packaging process is worthy of in-depth analysis. Proper design of the thermal management system of high-power LEDs will greatly reduce energy consumption and effectively utilize low-grade thermal energy.

Herein, a double-nozzle spray cooling system was proposed for 300 W high-power LEDs. The effect of nozzle configuration and the spray parameters including flow rate and nozzle-to-surface distance on the system were investigated experimentally. At the same time, in order to accurately explore the temperature distribution and junction temperature of LEDs chips in spray cooling, a detailed three-dimensional numerical simulation was carried out.

2. Experimental setup and methodology

2.1. LEDs module

In this work, the 300 W blue LEDs (SP100-I6BB-100, Shenzhen SkyBright Optoelectronics) was chosen to be tested as shown in Fig. 1a. This LEDs module has 100 chips arranged in a square array with an area of 20 mm × 20 mm, and the maximum input electric power of each chip is 3 W. The maximum input electric power of the LEDs module can reach 300 W under good heat dissipation conditions.

The optical performance was obtained by an integrating sphere system (ATA-1000, Everfine) and the relationship between the light efficiency of the LEDs and the input current at different temperatures was shown in Fig. 1b. The results show that as the temperature increases, the light efficiency will gradually decrease. And the light power accounts for about 30%-40% of the input electric power, while the heat power accounts for about 60%-70% of the input electric power as shown in Fig. 1c.

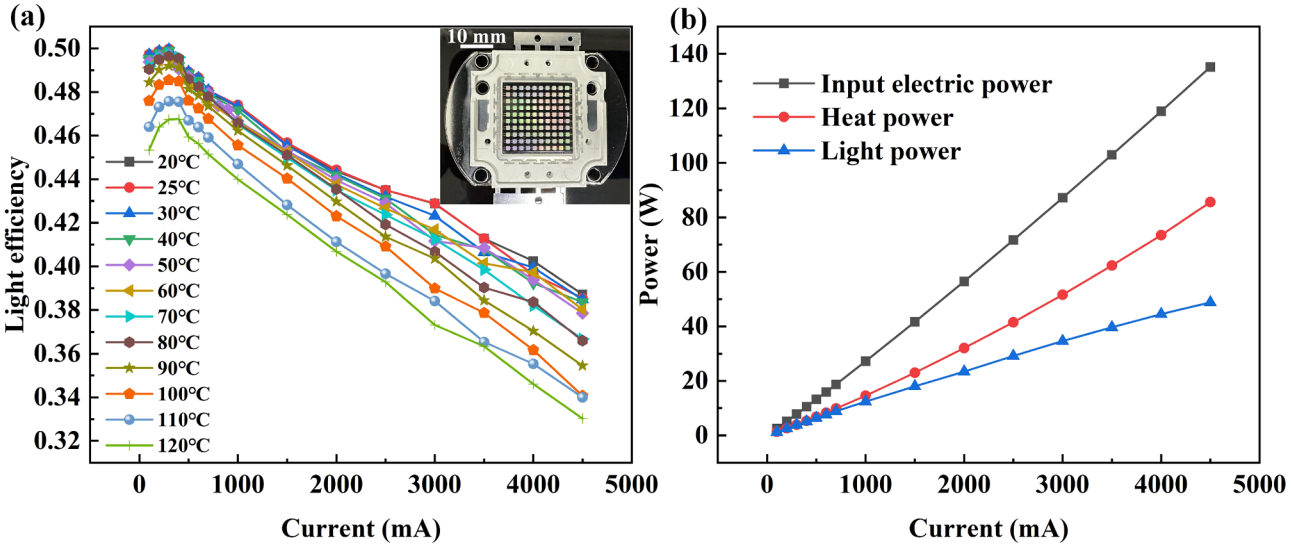

Fig. 1. (a) The relationship between light efficiency and driven current under various temperatures, (b) The input electric power, light power, and heat power of the LEDs module under various driven currents.

2.2. Spray cooling system

The experiments were conducted in an open system. Fig. 2 shows the schematic diagram of the apparatus used in the spray cooling experimental setup. Four parts consist of the whole experimental system, namely, the flow loop circuit system, the high-power LEDs testing framework, the data acquisition system, and the visualization system.

The deionized water was chosen as the working coolant stored in the reservoir (DC-2010, temperature control range: −20-100 °C, accuracy: ±0.1%, Zhulan). A gear pump (NP400, 24 V-400 W, Suofu) was used to drive the deionized water onto the heated surface through a solid cone pressure nozzle (B1/4TT-SS + TG-SS0.3, Spraying Systems Company). Under the experimental condition of double nozzle, there were two nozzles arranged side by side parallelly to the horizontal orientation, 25 mm apart. The flow rate of the nozzle and the pressure drop across nozzle were measured by the flow meter (CX-P2-F, measuring range: 3–300 mL/min, accuracy: ±0.5%, Gnflowmeter) and pressure gauge (SIN-Y190, measuring range: 0–5 MPa, accuracy: ±1%, Sinomeasure) respectively.

In order to get the thermal management capacity of spray cooling and prevent the LEDs from short-circuit, a LEDs testing framework was designed as shown in Fig. 3. The high-power LEDs was assembly integrated with a copper spreader and protected by a framework made by PEEK (Polyether-ether-ketone). Also, the excellent thermal insulation ability of PEEK minimized heat loss. The thermal grease (OT-201, Omega Engineering) was used to decrease the thermal contact resistance between the LEDs heat sink and the spreader. Furthermore, seven K-type thermocouples (TT-K-36, ETA) were embedded in the spreader to measure the heat flux and temperature distribution accurately, as shown in Fig. 3b. In order to clearly show the lateral distribution of the thermocouples, the cross-section view at A-A plane is shown in Fig. 3c. The insertion depth of the unshown four thermocouples is the same as the three thermocouples shown in Fig. 3c. A programmable DC power supply (FTP032-30016, Faith) was employed to provide stable input electric power for high-power LEDs. The inlet coolant temperature and ambient temperature were given by the thermocouples placed in the reservoir and spray chamber. A data acquisition instrument (Keithley 2700) was used to collect, record, and display the signals of all thermocouples.

A visualization system was built to observe and assess the performance of the spray cooling system. A high-speed camera (SA2 120 K, Photron) was used to obtain the spray morphology. The Sauter mean diameter (SMD, d_{32}) and the droplet velocity were measured by using Phase Doppler Interferometer.

2.3. Data analysis method and uncertainty analysis

The one-dimensional Fourier's law of heat conduction can be applied and the heat flux is estimated at the middle of the spreader as:

$$q'' = -k\frac{\Delta T(y)}{\Delta y} \tag{1}$$

$\Delta T(y)/\Delta y$ is the temperature gradient fitted by three thermocouples T_{21}, T_{22}, and T_{23}.

The substrate temperature T_{s1} and the surface temperature T_{s2} are estimated from the temperature of T_{21} and T_{23}, respectively.

$$T_{s1} = T_{21} - \frac{q''y_1}{k} \tag{2}$$

$$T_{s2} = T_{23} - \frac{q''y_2}{k} \tag{3}$$

The heat transfer coefficient h can be evaluated as:

$$h = \frac{q''}{T_{s2} - T_{in}} \tag{4}$$

The uncertainties of the thermocouples and thermocouple position are about ± 0.8 °C and ± 0.1 mm. Based on error transfer functions on this experimental bench, the uncertainties of surface temperature, heat flux, and heat transfer coefficient can be calculated by [34]:

$$\sigma_y = \sqrt{\sum_{i=1}^{n}\left(\frac{\partial f}{\partial x_i}\right)^2 \sigma_{x_i}^2} \tag{5}$$

The results showed that the maximum uncertainties of heat flux, surface temperature, and heat transfer coefficient are 2.1%, ±3.2%, and ± 2.2%, respectively.

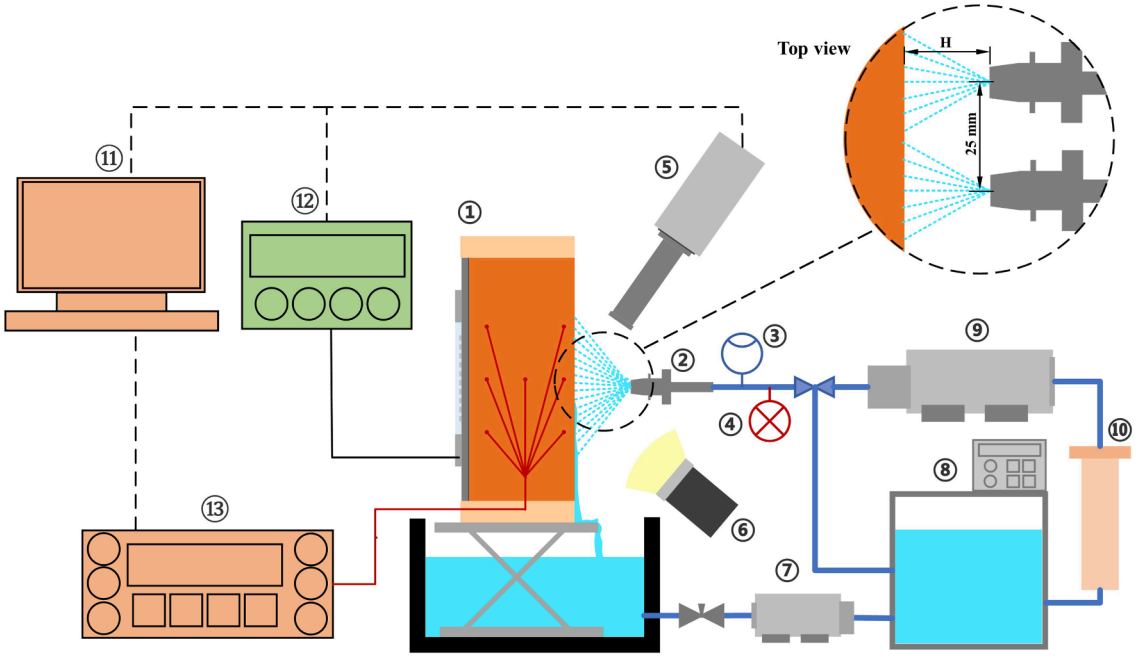

Fig. 2. Schematic layout of the experimental setup: 1. The LEDs testing device, 2. Nozzle, 3. Pressure gauge, 4. Flow rate gauge, 5. A high-speed camera, 6. Light source, 7. Diaphragm pump, 8. Reservoir, 9. Gear pump, 10. Filter, 11. Computer, 12. Data acquisition system, 13. DC power.

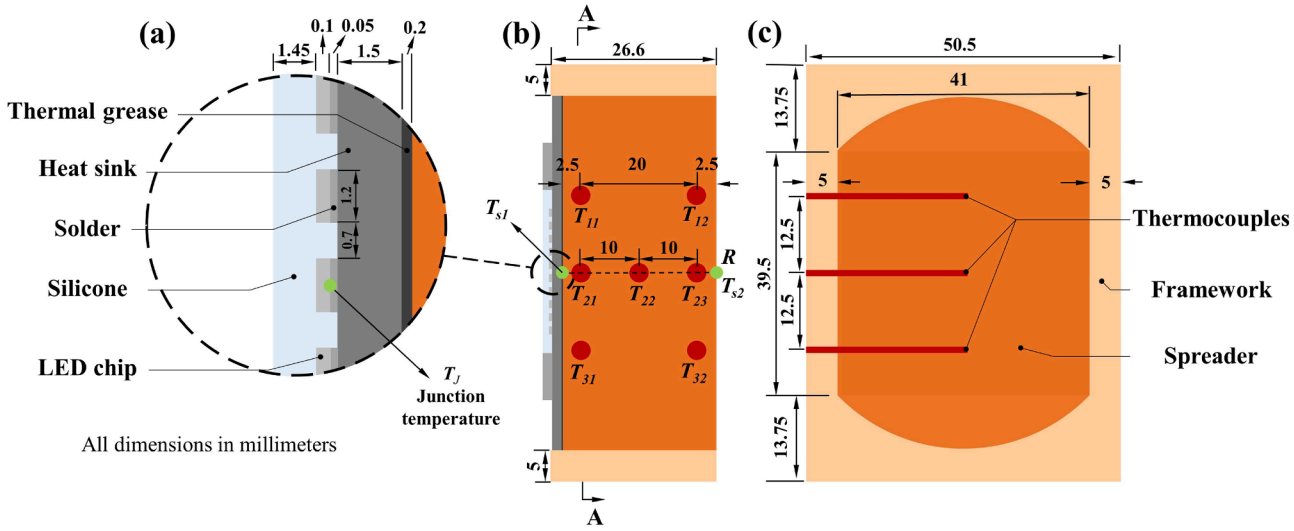

Fig. 3. High-power LEDs assembly, (a) The detailed structure of LEDs, (b) The cross-sectional view with the location of thermocouples, (c) The view at A-A plane.

2.4. Simulation details

The COMSOL Multiphysics® Software had been employed in this study and it is a supplement to the experiments where the junction temperature is hard to obtain. The simulation model was shown in Fig. 3 and Fig. 4. The thermal conductivity of materials used in the simulation is shown in Table 1. The results of the numerical simulation were obtained under steady state. The governing equations are:

$$\rho C_p \frac{\partial T}{\partial t} + \nabla \cdot q'' = Q \tag{6}$$

$$q'' = -k\nabla T = h(T - T_{in}) \tag{7}$$

The boundary conditions and assumptions used in the simulation analysis are mentioned below:

(1) A constant heat transfer coefficient can be applied to the target surface as a boundary condition in the simulation. Here the heat transfer coefficient is the heat transfer coefficient of the target surface derived from the results of experiments.

Table 1
Thermal conductivity of materials used in the simulation.

	Materials	Thermal conductivity (W/m·K)
Spreader	Copper	398
Heat sink	Copper	398
Framework	Peek	0.29
Thermal grease	Silicone	16
Solder	H20E	29
LEDs chip	GaP, GaAlAs, GaAs, GaN	65.6
Encapsulation layer	PDMS	0.15

(2) Heat dissipation of thermal radiation is ignored, and the heat is mainly lost through the surface of the copper block in the way of convection heat transfer. The heat transfer coefficient of other surfaces exposed to environment is set to 10 W/m^2·K due to the natural convection.
(3) Blue LEDs module was used in this work. The light absorption of silica gel can be ignored.

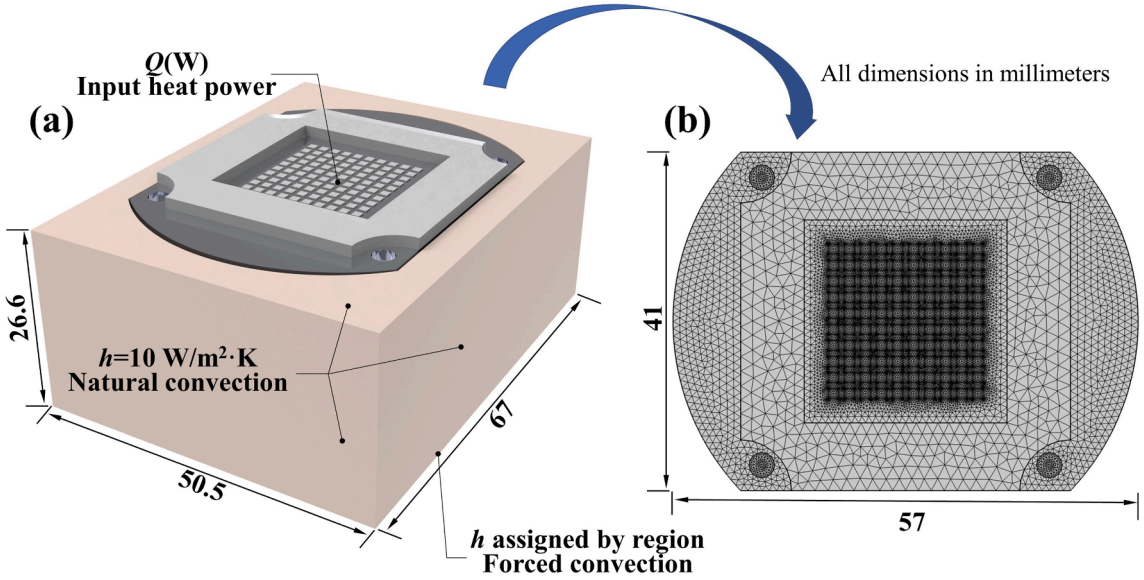

Fig. 4. (a) Computational domain used for the simulation, (b) Nature of meshing the LEDs module used for the simulation.

(4) The heat power of each chip is uniform which is the total heat power divided by the volume of the chip.
(5) The thermal properties (thermal conductivity, heat capacity, and density) of all materials are assumed to be uniform, isotropic, and independent of temperature.
(6) The material contact through the interface is considered perfect (no air gap and surface roughness).

In order to validate the proposed simulation model, the numerical models of Abdelmlek et al. and Sahu et al. [33] are compared with our model, as shown in Fig. 5. The maximum difference in junction temperature is about 4.8%. Grid independence test is conducted under different input electric power and three different grid sizes are chosen, namely finer, extra fine, and extremely fine. The total number of grids is 1786541, 3538358, and 9072035, respectively. The maximum temperature deviation between the grid size of finer and extra fine is 0.01 °C while there is no temperature deviation between the grid size of extra fine and extremely fine. Based on the accuracy and the simulation times, the finer size is selected for the remainder of the study.

3. Results and discussions

3.1. Characterization of nozzle

Spray cooling removes the heat from the target surface by employing the droplet clusters ejected from the nozzle. The characteristics of the droplet and spray significantly influence the performance of the spray cooling. As mentioned before, the characterization of nozzle is conducted in this study.

The spray morphology of different flow rates is displayed in Fig. 6 and each set of image includes two pictures. The picture on the left is the overall morphology of the spray, and the picture on the right is the morphology near the center line of the nozzle outlet. The value of different parameters obtained by our characterization is shown in Table 2.

3.2. Heat transfer analysis

As shown in Fig. 3, seven thermocouples are embedded in the copper block to evaluate the thermal management capacity of spray cooling such as heat transfer coefficient (h), substrate temperature (T_{s1}), surface temperature (T_{s2}), and temperature distribution. In this study, the effect of flow rate (Q) and nozzle-to-surface distance (H) on the spray cooling system are investigated. The performance of single- and double-nozzle spray cooling system are compared as three different expressions are used to identify different experimental conditions, namely "Double-nozzle-1", "Double-nozzle-2", and "Single-nozzle". The flow rate of "Double-nozzle-1" and "Single-nozzle" refers to the flow rate of each nozzle while the flow rate of "Double-nozzle-2" refers to the total flow rate of two nozzles.

To verify the rationality of the experimental data and the reliability of the experimental apparatus, the h obtained in the present study is compared with the reported value in the published literature [33,35,36] as shown in Fig. 7. The experiments are conducted with the input electric power of 300 W for comparison based on H of 20 mm and 30

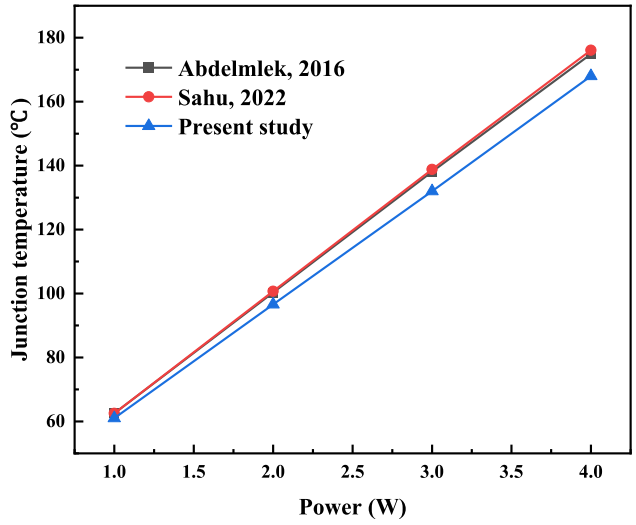

Fig. 5. Validation plot of previous numerical studies for the simulation model.

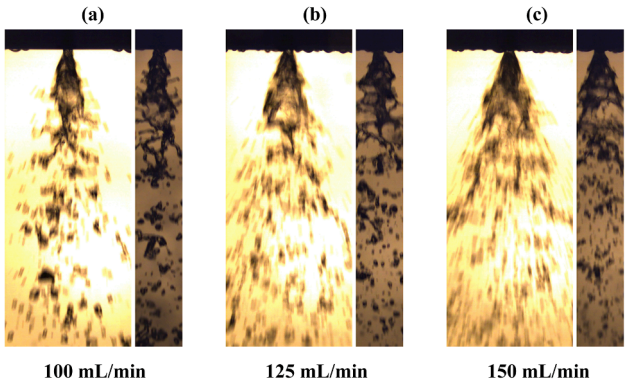

Fig. 6. Photographic details of spray morphology of different flow rates, (a) flow rate of 100 mL/min, (b) flow rate of 125 mL/min, (c) flow rate of 150 mL/min.

Table 2
Characterization of nozzle.

Nozzle-to-surface distance (mm)	Flow rate (mL/min)	Sauter mean diameter (μm)	Velocity at the center line (m/s)	Pressure drop across nozzle (Mpa)	Spray angle (°)
10	100	264.31	3.35	0.04	34.0
20	100	255.41	2.98	0.04	34.0
30	100	259.65	1.47	0.04	34.0
10	125	217.59	3.74	0.06	44.7
10	150	188.24	3.94	0.09	57.6
30	125	99.50	1.76	0.06	44.7
30	150	101.70	1.65	0.09	57.6

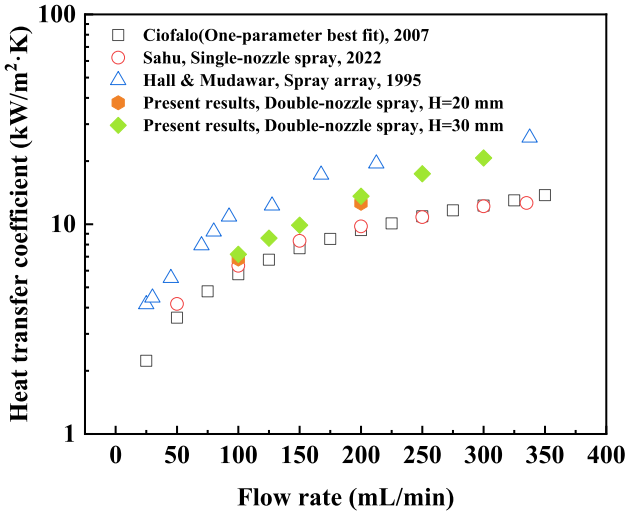

Fig. 7. Heat transfer coefficient h at stagnation point (R) in comparison with the previous studies [33,35,36].

mm. It can be drawn from Fig. 7 that the results are in good agreement with previous experiments, no matter the experiments of the single-phase spray cooling (Ciofalo et al. and Hall and Mudawar) or the experiments of the thermal management of LED (Sahu et al.). Moreover, the present study of double-nozzle spray cooling shows better heat dissipation capacity than single-nozzle spray cooling (Ciofalo et al. and Sahu et al.) while it is weaker than the spray array (Hall and Mudawar).

3.2.1. Effect of nozzle configuration and flow rate

There is a consensus that the flow rate (Q) is one of the most important hydrodynamic parameters in the spray cooling. The flow rate is controlled as 100 mL/min, 125 mL/min, and 150 mL/min in this study and two different nozzle configurations are investigated, namely double nozzle and single nozzle.

Fig. 8 gives out the thermo-hydraulic evaluation based on different nozzle configurations and flow rates. The h increases with the Q and the h remains similar around different input electric power under each nozzle configuration as shown in Fig. 8a. The h of Double-nozzle-1 is larger than Single-nozzle and Double-nozzle-2 over the entire input electric power range. At the Q of 150 mL/min, there is a 64.9% growth in h when the experimental condition changes from Single-nozzle to Double-nozzle-1 and a 113.8% growth in h when it changes from Double-nozzle-2 to Double-nozzle-1. Fig. 8b shows that T_{s1} decreases with the increase of Q. The T_{s1} of Double-nozzle-1 is lower than the T_{s1} of Double-nozzle-2 and Single-nozzle. At the maximum input electric power of 300 W, the highest h reaches 20.7 kW/m^2·K and the lowest T_{s1} reaches 50.3 °C.

Double-nozzle-1 has a larger total flow rate than Double-nozzle-2 and Single-nozzle. Larger Q refers that more coolant can reach the target surface and the droplet velocity is faster which can be proved by the characterization of the nozzle. The faster droplet velocity makes it easier to break the boundary layer and provides timely fluid replenishment to form new liquid membrane for stronger heat dissipation. However, although Double-nozzle-2 has the same Q as Single-nozzle, the Q of each nozzle of Double-nozzle-2 is half of Single-nozzle. The lower flow rate will lead to smaller droplet velocity, larger droplet size, and smaller spray covering area according to the characterization of nozzle. Smaller droplet velocity and larger droplet size will lead to a thicker liquid membrane and a slower rate of liquid removal which are unfavourable for heat dissipation. Furthermore, as for double nozzle, the smaller spray covering area of each nozzle will lead to a separated state. There will be flow interactions and blockage between neighboring sprays which lead to worse heat dissipation capacity. Therefore, under the same total flow rate, the performance of Double-nozzle-2 is not as good as that of Single-nozzle.

Compared to Single-nozzle, Double-nozzle-1 can give larger h in a greater area. Fig. 9 compares the temperature at T_{11}, T_{21}, and T_{31} under different experimental conditions. At the Q of 100 mL/min and 150 mL/min, the T_{s1} of Double-nozzle-1 is lower than Double-nozzle-2 and Single-nozzle. The temperature of T_{21} is higher than T_{11} and T_{31} which are similar to each other. LEDs is a temperature-sensitive optical device, and if any chip burns out, the module will be invalid. Therefore, the smaller the temperature difference between thermocouples in the same height, namely the better the temperature uniformity, the better the thermal management capacity.

In order to visualize the temperature non-uniformity ΔT_{uni}, the standard deviation of the temperature variation has been calculated as

$$\Delta T_{\text{uni}} = S = \sqrt{\frac{\sum_{i=1}^{3}(T_{i1} - \overline{T})^2}{2}} \tag{8}$$

Fig. 10 shows that ΔT_{uni} versus input electric power under different nozzle configurations and Q. As for Double-nozzle-1 and Double-nozzle-2, the ΔT_{uni} are similar among different Q. However, the larger the Q, the larger the ΔT_{uni} for Single-nozzle. Combined with the characterization of nozzle, it can be found that the increase of Q leads to the increase of spray angle. As a result, the spray impact area will increase at the same H. The mean volumetric flux ($\overline{Q}''$) which is defined by dividing the total volume flow rate of the spray by the portion of the surface directly impacted by the spray are 6.2×10^{-3}, 4.4×10^{-3}, and 2.9×10^{-3} m^3/s·m^2 for 100, 125, and 150 mL/min. More specifically, the decrease of $\overline{Q}''$ will lower the heat dissipation capacity of the central area under a large Q, resulting in higher temperature and larger temperature non-uniformity.

In addition, the ΔT_{uni} of double-nozzle configuration is larger than single-nozzle configuration. The reason is not duplicating for Double-nozzle-1 and Double-nozzle-2. The temperature distribution of the LEDs module of Double-nozzle-1 is lower than Single-nozzle, and it of Single-nozzle is lower than Double-nozzle-2. As for lower temperature distribution, it is more difficult to achieve a uniform temperature dis-

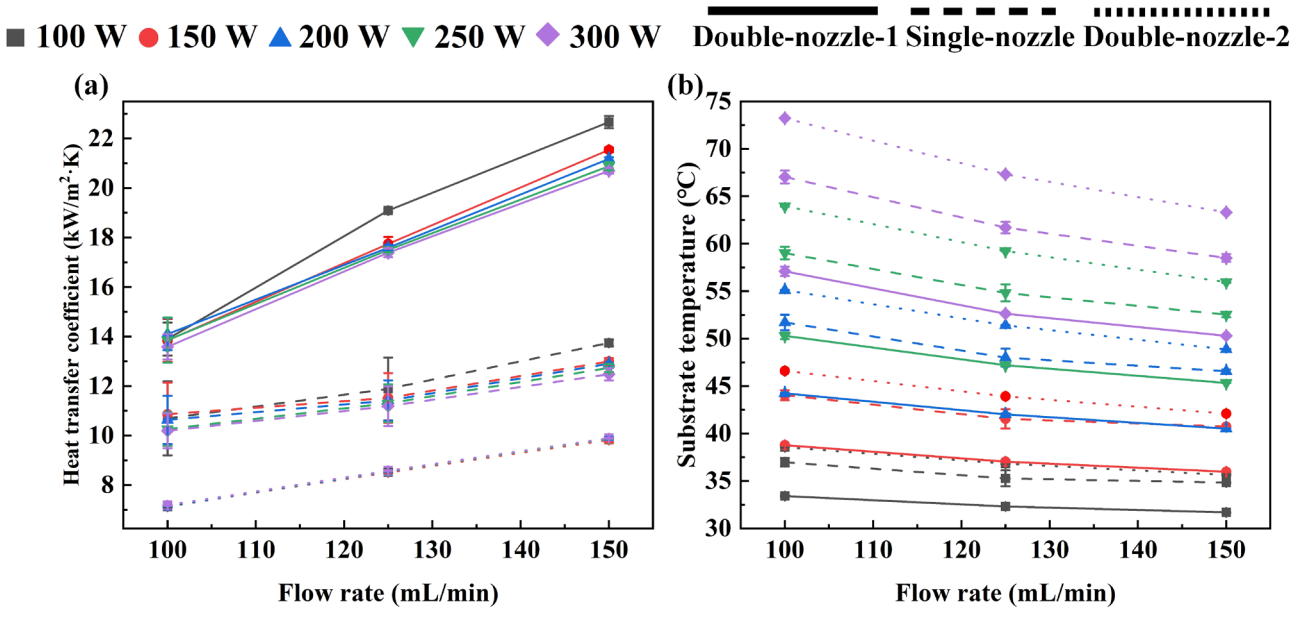

Fig. 8. Thermo-hydraulic evaluation of different nozzle configurations, (a) Heat transfer coefficient h versus flow rate Q, (b) Substrate temperature T_{s1} versus flow rate Q.

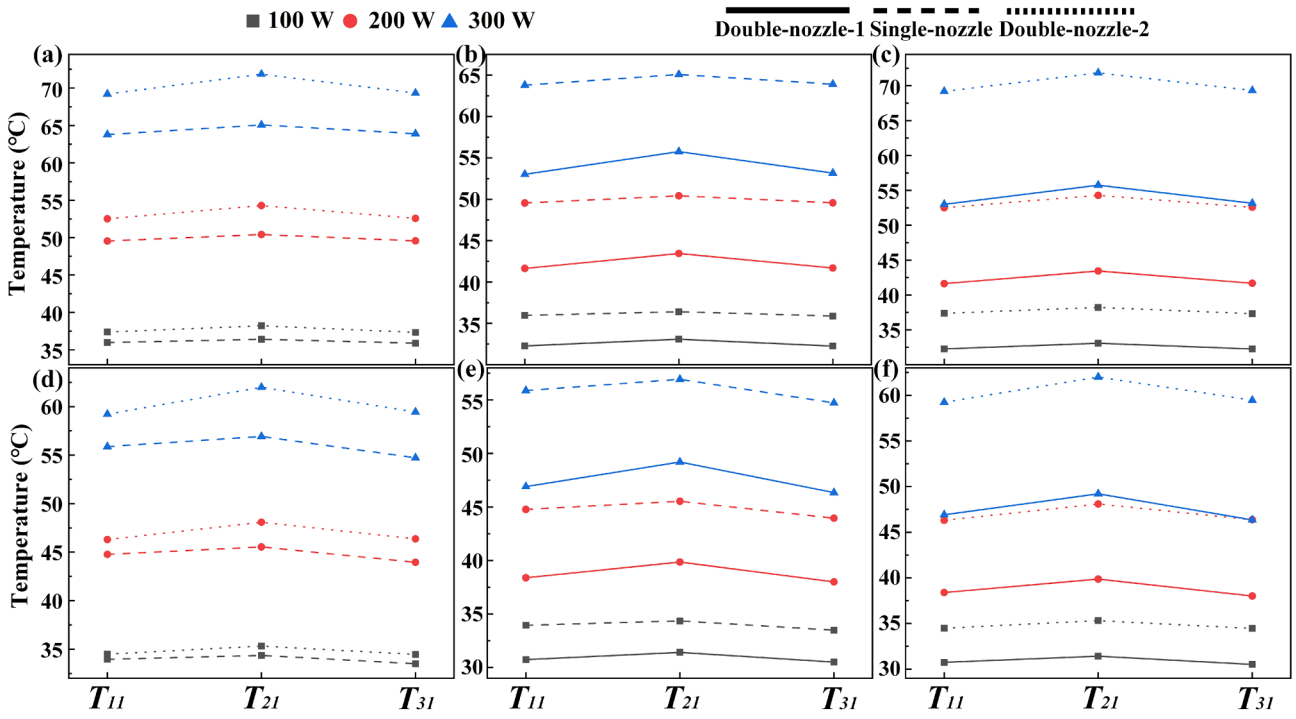

Fig. 9. Temperature of T_{11}, T_{21}, and T_{31} with different flow rates and input electric power, (a) Comparison of Single-nozzle and Double-nozzle-2 at Q of 100 mL/min, (b) Comparison of Single-nozzle and Double-nozzle-1 at Q of 100 mL/min, (c) Comparison of Double-nozzle-1 and Double-nozzle-2 at Q of 100 mL/min, (d) Comparison of Single-nozzle and Double-nozzle-2 at Q of 150 mL/min, (e) Comparison of Single-nozzle and Double-nozzle-1 at Q of 150 mL/min, (f) Comparison of Double-nozzle-1 and Double-nozzle-2 at Q of 150 mL/min.

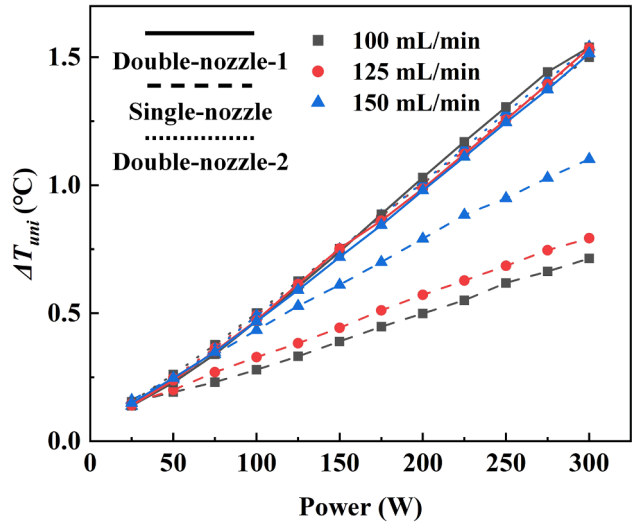

Fig. 10. Temperature non-uniformity versus input electric power with different nozzle configurations and flow rates.

tribution inside the module. Meanwhile, the lack of heat dissipation capacity can also lead to a non-uniform temperature distribution, just like Double-nozzle-2. Therefore, the judgement criterion of temperature non-uniformity is worthy of further discussion.

3.2.2. *Effect of nozzle-to-surface distance*

The packaging constrains and the trend towards miniaturization of electronic devices both limit the volume of high-power LEDs. Exploring the effect of nozzle-to-surface distance (H) on spray cooling of high-power LEDs can provide guidance for the design of the thermal management system. The H is chosen as 10, 20, and 30 mm. All experiments are conducted based on Double-nozzle-1 and Q of 100 mL/min.

The thermal evaluation is plotted in Fig. 11. The h increases with the increase of the H and it remains similar between different input electric power. The T_{s1} goes down with the increase of the H. In short, the farther the H, the better the heat dissipation capacity. As shown in Table 2, the droplet velocity is lower at the farther H. Nevertheless, the surface area directly impacted by the spray is larger at the farther H. The heat transfer mechanism is different in the direct impact area and the non-direct impact area. In the direct impact area, high-speed droplets impact the surface, break the boundary layer, take away the heat, and replenish the liquid membrane timely. In the non-direct impact area, forced convection of coolant is the main mechanism to carry away the heat load while it is inefficient. Hence, the size of the direct impact area is a more important factor than droplet velocity in spray cooling.

The temperature non-uniformity evaluation based on different H is shown in Fig. 12. The temperature of T_{21} is higher than T_{11} and T_{31} which are similar with each other as shown in Fig. 12a. Fig. 12b gives the ΔT_{uni} versus input electric power under different H. The ΔT_{uni} is similar among H of 10 and 20 mm While the ΔT_{uni} is smaller at H of 30 mm. The reason why ΔT_{uni} goes up slightly when H are 10 and 20 mm is that the lower the H, the larger the $\overline{Q}''$ and the droplet velocity while the direct impact area is smaller. As a result, the huge difference in heat dissipation capacity between direct impact area and non-direct impact area will cause a larger ΔT_{uni}. But in general, as shown in Fig. 12b, ΔT_{uni} is not sensitive to the changes of H.

3.3. *Simulation analysis*

As mentioned before, the junction temperature (T_J) is the critical indicator of LEDs module which is incapable to be measured by the thermocouple directly. The simulation is employed to obtain the T_J of the center chip column.

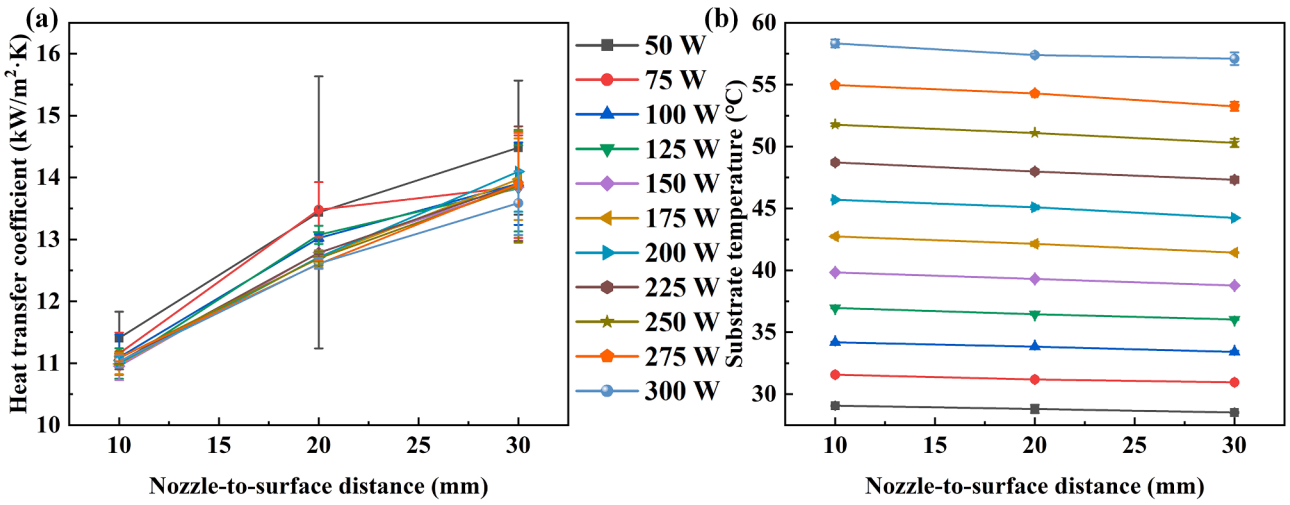

Fig. 11. Thermal evaluation of Double-nozzle-1 at the flow rate of 100 mL/min, (a) Heat transfer coefficient h versus nozzle-to-surface distance H, (b) Substrate temperature T_{s1} versus nozzle-to-surface distance H.

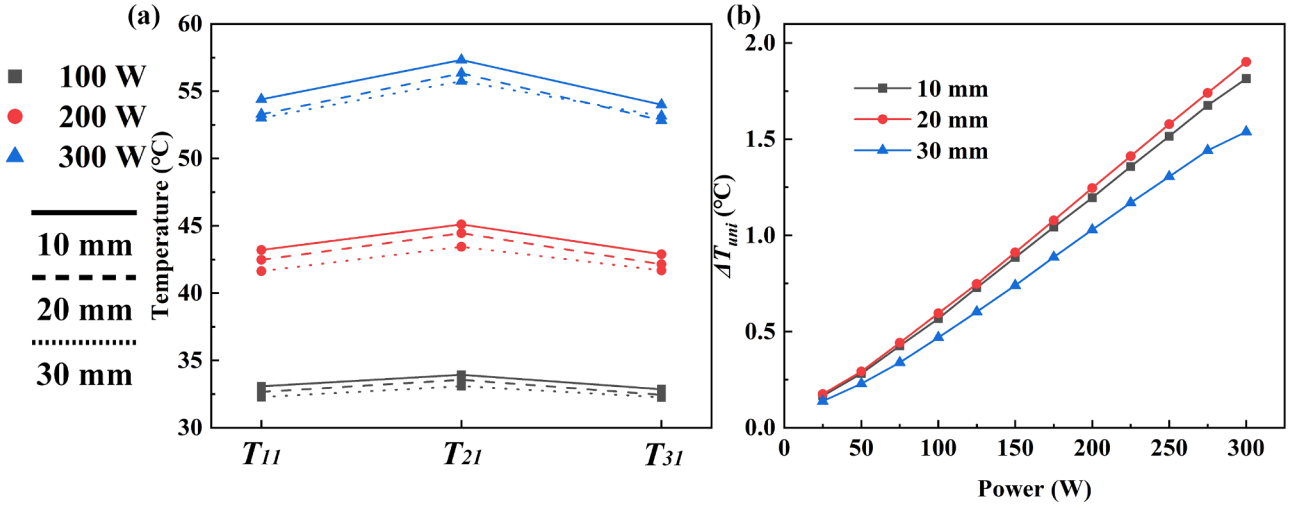

Fig. 12. Temperature non-uniformity evaluation of Double-nozzle-1 at Q of 100 mL/min, (a) Temperature of T_{11}, T_{21}, and T_{31} with different nozzle-to-surface distance H, (b) Temperature non-uniformity versus input electric power with different nozzle-to-surface distance H.

3.3.1. Validation study

It can be drawn from the previous analysis that the heat dissipation capacity of spray cooling is different in the direct impact area and the non-direct impact area. In the simulation, we adopt the method of assigning heat transfer coefficient by region to make the simulation more accurate. The surface of the copper block exposed to the environment is divided into the direct impact area and the non-direct impact area of which the sizes are determined by the spray angle, H, and D. The nozzle configuration of single-nozzle and double-nozzle are both validated at Q of 150 mL/min among the whole range of input electric power. Fig. 13 expresses the comparison of steady-state temperature between the experiment and the simulation at different thermocouple positions. The data of experiment and simulation are in good agreement with each other.

3.3.2. Estimation of junction temperature

The chips are distributed in a square array in the LEDs module. Thus, there will be heat accumulation in the center of LEDs module and the T_J of chip column at the center are chosen for analysis when the input electric power is 300 W. Fig. 14a is the diagram of different chip locations. The T_J distribution of Double-nozzle-1 and Single-nozzle at different Q are shown in Fig. 14b. Fig. 14c compares T_J of different H of Double-nozzle-1. The T_J distribution of Double-nozzle-1 is lower than it of Single-nozzle and Fig. 14b and Fig. 14c both prove that the T_J is symmetrically distributed around the LEDs center. As mentioned above, the temperature sensitivity of the LEDs module causes it to be completely damaged due to local overheating. Hence, the temperature of the center chip is analyzed. The result shows that when Q is 150 mL/min, Double-nozzle-1 achieves the lowest T_J of the center chip, which is 85 °C. Under the same condition, the value of T_J is 94 °C of Single-nozzle, which is 10% higher than that of Double-nozzle-1. Additionally, the farther the H, the lower the T_J. The decrease of T_J resulting from increasing the Q and nozzle numbers is greater than that by increasing the H. When H changes from 10 mm to 20 mm, the highest T_J decrease by 1.7% while it is only 0.5% when H changes from 20 mm to 30 mm. The results show the consistency of the effect of H on h, ΔT_{uni}, and T_J. In other words, the effect of changing H on the heat transfer capacity of spray cooling is very limited. However, this also implies that adjusting H to fit the packaging constrain has greater application potential.

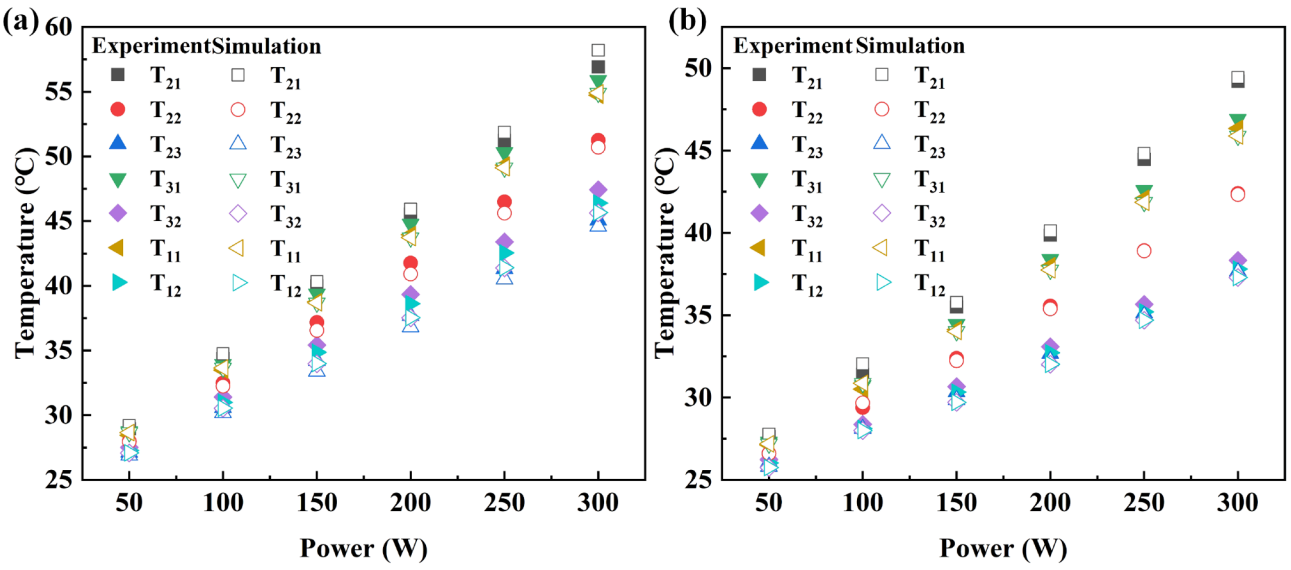

Fig. 13. Steady-state temperature at different positions for various input electric power at flow rate of 150 mL/min, (a) Single-nozzle, (b) Double-nozzle-1.

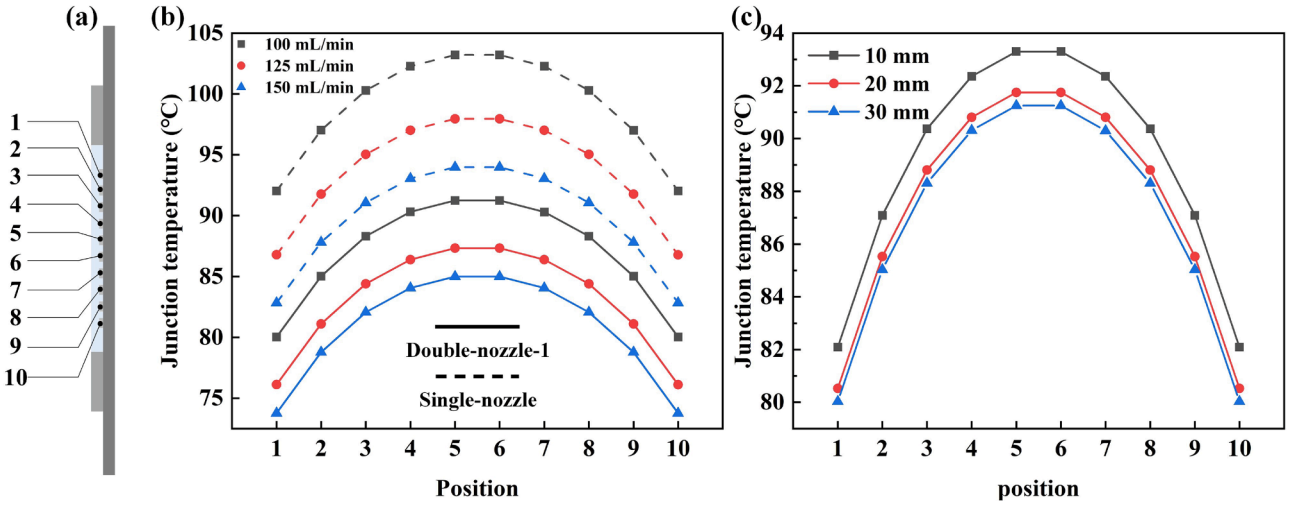

Fig. 14. Junction temperature T_J of high-power LEDs under the input electric power of 300 W, (a) Cross-sectional view of LEDs module at the center chip column, (b) Comparison of Double-nozzle-1 and Single-nozzle at different flow rates, (c) Comparison of different nozzle-to-surface distance H of Double-nozzle-1.

4. Conclusion

We present a high-performance spray cooling system for co-designing nozzle configuration and electronics for thermal management, and demonstrate it on high-power LEDs. The double-nozzle configuration greatly enhances the heat dissipation capacity and achieves a heat transfer coefficient of 20.7 kW/m^2·K which is 65.8% higher than that of single-nozzle at the maximum nominal power of LEDs. The junction temperature of center chip can also be controlled to 85 °C which is 10% lower than that of single-nozzle. Meanwhile, the results show that a larger flow rate cannot lead to better temperature uniformity for the decrease of mean volumetric flux of single-nozzle. And it is more intractable to achieve uniform temperature and assess temperature non-uniformity while the module's temperature is low.

Nozzle configurations such as the separation between nozzles and the inclination of the nozzle require further investigation in spray cooling. For instance, an array spray arrangement can offer better cooling efficiency and require less coolant which is beneficial to reduce the package size of electronics, while it will make the system more complex and deteriorate the heat transfer performance in the spray overlap area. Co-design of nozzle configurations and electronics for spray cooling system can provide the optimal thermal management solution for electronics. This may aid in solving critical challenges in spray cooling applications in electronics, as well as enabling energy-efficient cooling and utilization of low-grade thermal energy.

CRediT authorship contribution statement

Linyi Xiang: Conceptualization, Methodology, Software, Formal analysis, Investigation, Writing – original draft, Writing – review & editing. **Yanhua Cheng:** Investigation, Writing – review & editing. **Xingjian Yu:** Conceptualization, Investigation. **Yiwen Fan:** Methodology, Resources. **Xuan Yang:** Software, Validation. **Xinfeng Zhang:** Methodology. **Bin Xie:** Writing – review & editing. **Xiaobing Luo:** Project administration, Funding acquisition, Writing – review & editing.

Declaration of Competing Interest

The authors declare that they have no known competing financial interests or personal relationships that could have appeared to influence

the work reported in this paper.

Data availability

Data will be made available on request.

Acknowledgments

This research is supported by the National Natural Science Foundation of China (52106089 and 52076087) and the Science and Technology Program of Hubei Province (2021BLB176).

References

[1] B. Xie, Y.J. Wang, H.C. Liu, J.L. Ma, S.L. Zhou, X.J. Yu, W. Lan, K. Wang, R. Hu, X. B. Luo, Targeting cooling for quantum dots by 57.3℃ with air-bubbles-assembled three-dimensional hexagonal boron nitride heat dissipation networks, Chem. Eng. J. 427 (2022), 130958.
[2] X.J. Yu, L.Y. Xiang, S.L. Zhou, N.Q. Pei, X.B. Luo, Effect of refractive index of packaging materials on the light extraction efficiency of COB-LEDs with millilens array, Appl. Opt. 60 (2) (2021) 306–311.
[3] X.B. Luo, R. Hu, S. Liu, K. Wang, Heat and fluid flow in high-power LED packaging and applications, Prog. Energy Combust. Sci. 56 (2016) 1–32.
[4] M. Hamidnia, Y. Luo, X.D. Wang, Application of micro/nano technology for thermal management of high power LED packaging - A review, Appl. Therm. Eng. 145 (2018) 637–651.
[5] L.Y. Xiang, R. Hu, Liquid directional steering, Matter 5 (1) (2022) 13–15.
[6] X. Yang, S.L. Zhou, B. Xie, X.J. Yu, X.F. Zhang, L.Y. Xiang, K. Wang, X.B. Luo, Enhancing Heat Dissipation of Quantum Dots in High-Power White LEDs by Thermally Conductive Composites Annular Fins, IEEE Electr. Device L. 42 (8) (2021) 1204–1207.
[7] L. Branko, K. Roy, A very high flux in microchannel heat exchanger for cooling of semi-conductor laser diode arrays, Proc. IEEE Trans. Components - Part B 19 (1996) 444–451.
[8] S. Khandekar, G. Sahu, K. Muralidhar, E.Y. Gatapova, O.A. Kabov, R. Hu, X.B. Luo, L. Zhao, Cooling of high-power LEDs by liquid sprays: Challenges and prospects, Appl. Therm. Eng. 184 (2021), 115640.
[9] E. Tamdogan, M. Arik, Natural convection immersion cooling with enhanced optical performance of light-emitting diode systems, J. Electron. Packag. Trans. ASME. 137 (2015) 1–8.
[10] P. Kumar, G. Sahu, D. Chatterjee, S. Khandekar, Copper wick based loop heat pipe for thermal management of a high-power LED module, Appl. Therm. Eng. 211 (2022), 118459.
[11] X. Luo, R. Hu, T. Guo, X. Zhu, W. Chen, Z. Mao, S. Liu, Low thermal resistance LED light source with vapor chamber coupled fin heat sink, in: 2010 Proceedings 60th Electronic Components and Technology Conference (ECTC), (2010) 1347-1352.
[12] C. Xiao, H. Liao, Y. Wang, J. Li, W. Zhu, A novel automated heat-pipe cooling device for high-power LEDs, Appl. Therm. Eng. 111 (2017) 1320–1329.
[13] X.F. Zhang, B. Xie, S.L. Zhou, X. Yang, Y.W. Fan, R. Hu, X.B. Luo, Radially oriented functional thermal materials prepared by flow field-driven self-assembly strategy, Nano Energy 104 (2022), 107986.
[14] I. Mudawar, Recent advances in high-flux, two-phase thermal management, J. Thermal Sci. Eng. Appl. 5 (2013), 021012.
[15] A.C. Kheirabadi, D. Groulx, Cooling of server electronics: A design review of existing technology, Appl. Therm. Eng. 105 (2016) 622–638.
[16] B. Agostini, M. Fabbri, J.E. Park, L. Wojtan, J.R. Thome, B. Michel, State of the art of high heat flux cooling technologies, Heat Transf. Eng. 28 (4) (2007) 258–281.
[17] J.-H. Seo, M.-Y. Lee, illuminance and heat transfer characteristics of high power LED cooling system with heat sink filled with ferrofluid, Appl. Therm. Eng. 143 (2018) 438–449.
[18] Y.C. Chung, H.H. Chung, Y.H. Lee, L.Q. Yang, Heat dissipation and electrical conduction of an LED by using a microfluidic channel with a graphene solution, Appl. Therm. Eng. 175 (2020), 115383.
[19] X. Lin, S. Mo, B. Mo, L. Jia, Y. Chen, Z. Cheng, Thermal management of high-power LED based on thermoelectric cooler and nanofluid-cooled microchannel heat sink, Appl. Therm. Eng. 172 (2020), 115165.
[20] M.W. Jeong, S.W. Jeon, S.H. Lee, Y. Kim, Effective heat dissipation and geometric optimization in an LED module with aluminum nitride (AlN) insulation plate, Appl. Therm. Eng. 76 (2015) 212–219.
[21] B. Ramos-Alvarado, B. Feng, G.P. Peterson, Comparison and optimization of single-phase liquid cooling devices for the heat dissipation of high-power LED arrays, Appl. Therm. Eng. 59 (2013) 648–659.
[22] X. Deng, Z. Luo, Z. Xia, W. Gong, L. Wang, Active-passive combined and closed-loop control for the thermal management of high-power LED based on a dual synthetic jet actuator, Energy Convers. Manage. 132 (2017) 207–212.
[23] X. Luo, W. Chen, R. Sun, S. Liu, Experimental and numerical investigation of a microjet-based cooling system for high power LEDs, Heat Transf. Eng. 29 (9) (2008) 774–781.
[24] E.Y. Gatapova, G. Sahu, S. Khandekar, R. Hu, Thermal management of high-power LED module with single-phase liquid jet array, Appl. Therm. Eng. 184 (2021), 116270.
[25] S. Liu, J. Yang, Z. Gan, X. Luo, Structural optimization of a microjet based cooling system for high power LEDs, Int. J. Therm. Sci. 47 (8) (2008) 1086–1095.
[26] J. Kim, Spray cooling heat transfer: The state of the art, Int. J. Heat. Fluid. Fl. 28 (2007) 753–767.
[27] G.T. Liang, I. Mudawar, Review of spray cooling- Part 1: Single-phase and nucleate boiling regimes, and critical heat flux, Int. J. Heat Mass Transf. 115 (2017) 1174–1205.
[28] L.Y. Xiang, X.J. Yu, T. Hong, X. Yang, B. Xie, R. Hu, X.B. Luo, Performance of spray cooling with vertical surface orientation: an experimental investigation, Appl. Therm. Eng. 219 (2023), 119434.
[29] J.X. Wang, W. Guo, K. Xiong, S.N. Wang, Review of aerospace-oriented spray cooling technology, Prog. Aerosp. Sci. 116 (2020), 100635.
[30] H.H. Dong, L. Ruan, Y. Wang, J. Yang, F.H. Liu, S.Q. Guo, Performance of air/spray cooling system for large-capacity and high-power-density motors, Appl. Therm. Eng. 192 (2021), 116925.
[31] S.R. Lei, Y. Shi, G.Y. Chen, A lithium-ion battery-thermal-management design based on phase-change-material thermal storage and spray cooling, Appl. Therm. Eng. 168 (2020), 114792.
[32] S.-S. Hsieh, Y.-F. Hsu, M.-L. Wang, A microspray-based cooling system for high powered LEDs, Energy Convers. Manage. 78 (2014) 338–346.
[33] G. Sahu, S. Khandekar, K. Muralidhar, Thermal characterization of spray impingement heat transfer over a High-Power LED module, Therm. Sci. Eng. Prog. 32 (2022), 101332.
[34] R.J. Moffat, contributions to the theory of single-sample uncertainty analysis, J. Fluids Eng. 104 (1982) 250–258.
[35] M. Ciofalo, A. Caronia, M. Di Liberto, S. Puleo, The Nukiyama curve in water spray cooling: Its derivation from temperature-time histories and its dependence on the quantities that characterize drop impact, Int. J. Heat Mass Transf. 50 (2007) 4948–4966.
[36] D.D. Hall, I. Mudawar, Experimental and numerical study of quenching complex-shaped metallic alloys with multiple, overlapping sprays, Int. J. Heat Mass Transf. 38 (1995) 1201–1216.